

Alignment Destabilizes Crystal Orders in Active Systems

Chen Huang¹, Leiming Chen², and Xiangjun Xing^{1,3,4*}

¹ *Wilczek Quantum Center, School of Physics and Astronomy, Shanghai Jiao Tong University, Shanghai 200240 China*

² *School of Materials Science and Physics, China University of Mining and Technology, Xuzhou, Jiangsu, 221116 China*

³ *T.D. Lee Institute, Shanghai Jiao Tong University, Shanghai 200240 China*

⁴ *Shanghai Research Center for Quantum Sciences, Shanghai 201315 China*

We combine numerical and analytical methods to study two dimensional active crystals formed by permanently linked swimmers and with two distinct alignment interactions. The system admits a stationary phase with quasi long range translational order, as well as a moving phase with quasi-long range velocity order. The translational order in the moving phase is significantly influenced by alignment interaction. For Vicsek-like alignment, the translational order is short-ranged, whereas the bond-orientational order is quasi-long ranged, implying a moving hexatic phase. For elasticity-based alignment, the translational order is quasi-long ranged parallel to the motion and short-ranged in perpendicular direction, whereas the bond orientational order is long-ranged. We also generalize these results to higher dimensions.

Introduction One of the most interesting and fundamental issues about active systems [1–6] is the stability of orders. According to the Mermin-Wagner theorem [7], two-dimensional (2D) equilibrium systems with continuous symmetry and short range interaction cannot exhibit not long range order (LRO). However, LRO was discovered in 2D polar active fluid both in simulation [8] and in hydrodynamic theory [9–11, 13]. This LRO is accompanied by super-diffusion and giant number fluctuations [2, 6, 11, 12], neither of which is seen in equilibrium systems with short range interactions. Many variants of Vicsek models with different particle polarity, alignments and exclusion [12–26] have been studied, a variety of novel phenomena have been discovered.

Dense active systems with repulsive interactions may also exhibit translational orders. Solid phases as well as fluid-solid phase separations have been repeatedly observed in active colloidal systems both experimentally [28–30] and numerically [27, 31–34]. In most of these works, there is no alignment interaction, and no visible collective motion. More recently, Weber *et. al.* [20][52] simulated a model active crystal with Vicsek-type alignment, and discovered a stationary phase with quasi-long range (QLR) translational order, as well as a phase of moving crystal domains separated by grain boundaries. Very recently, Maitra *et.al.* [35] studied an active generalization of nematic elastomer [38] with spontaneous breaking of rotational symmetry [36, 37], and found QLR translational orders in 2D. Their elastic energy contains a hidden rotational symmetry (and its resulting Goldstone modes) involving both shear deformation and orientational order, which are difficult to realize experimentally.

Regardless of many previous studies, it is not clear whether there exists a moving phase with certain translational order in active systems alignment interactions, if the soft-mode in Ref. [35] does not come into play. To address this interesting question, here we combine analytic and numerical approaches to study a model system of ac-

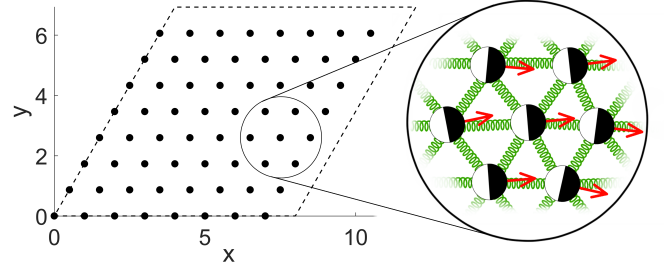


FIG. 1: Our simulation model. Swimmers are connected by springs and driven by active forces, shown as red arrows.

tive crystal consisting of 2D triangular array of swimmers linked permanently by springs. We introduce alignment interaction between neighboring swimmers that is either Vicsek-like (AD-I) or elasticity-based [39, 40] (AD-II). In the strong noise/weak alignment regime, we find a stationary phase with QLR translational order, which was also seen in Ref. [20]. In the weak noise/strong alignment regime we find a moving phase with QLR velocity order, and with the nature of translational order depending on the alignment. For Vicsek-like alignment (AD-I), the moving phase exhibits only short-range (SR) translational order and QLR bond orientational order, and hence should be identified with *moving hexatic phase*. For elasticity-based alignment (AD-II), the translational order is QLR along the moving direction, and SR in the perpendicular direction, whereas the bond-orientational order is LR. We generalize the model to higher dimensions, and show in active systems velocity alignment tends to destabilize crystal orders.

Simulation model As schematized in Fig. 1, our simulation model consists of a triangular array of swimmers connected permanently by harmonic springs. Each swimmer moves under the influences of elastic force, friction and noise, as well as active force. The position $\mathbf{r}_k(t)$ of k -th swimmer in the lab frame then obeys the following

over-damped Langevin equation:

$$\gamma \dot{\mathbf{r}}_k(t) = b \hat{n}(\theta_k) + \mathbf{F}_k(t) + \gamma \sqrt{2D} \hat{\xi}_k(t), \quad (1)$$

where γ is the friction coefficient, $\hat{n}(\theta_k) = (\cos \theta_k, \sin \theta_k)$ is the director of active force. The magnitude of active force b is assumed to be fixed in our model. The elastic force is

$$\mathbf{F}_k = \sum_{j \text{ n.n. } k} \kappa (|\mathbf{r}_k - \mathbf{r}_j| - a_0) \frac{\mathbf{r}_k - \mathbf{r}_j}{|\mathbf{r}_k - \mathbf{r}_j|}, \quad (2)$$

where the summation is over six nearest neighbors of swimmer k , whilst κ and a_0 are respectively the elastic constant and natural length of the springs. The last term of Eq. (1) is the random force, with $\hat{\xi}_k(t)$ the unit Gaussian white noise.

We consider two distinct alignment dynamics for the active forces. The first (AD-I) is Vicsek-like [41], with each swimmer trying to align its director of active force with its neighbors [53], subject to an internal noise:

$$\dot{\theta}_k(t) = d(\hat{n}(\theta_k) \times \langle \hat{n} \rangle_k) \cdot \hat{z} + \sqrt{2D_\theta} \eta_k(t), \quad (\text{AD-I})$$

where \hat{z} is the unit normal to the plane, $\langle \hat{n} \rangle_k \equiv \sum_{j \text{ n.n. } k} \hat{n}(\theta_j)/6$ the average director of all six nearest neighbors, and $\eta_k(t)$ is a unit Gaussian white noise.

The second alignment dynamics (AD-II) is elasticity-based [39, 40, 42], with each swimmer aligning its active force with the local elastic force, so as to reduce the local elastic energy:

$$\dot{\theta}_k(t) = c(\hat{n}(\theta_k) \times \mathbf{F}_k) \cdot \hat{z} + \sqrt{2D_\theta} \eta_k(t). \quad (\text{AD-II})$$

We use a rhombic cell with periodic boundary condition (c.f. Fig. 1), and numerically integrate the dynamic equations, Eqs. (1) and (AD-I) or (AD-II), using the first-order Euler-Maruyama scheme [43], with the time step $\Delta \tilde{t} = 10^{-3}$. Simulation details as well as the definitions of all dimensionless parameters, are given in Supplementary Information (SI) Sec. I.

We first determine the phase diagram by computing the velocity order parameter, defined as the steady state time average of magnitude of system-averaged active force $P = \langle |\frac{1}{N} \sum_k \hat{n}(\theta_k)| \rangle_t$, which is proportional to the velocity of collective motion. As shown in Fig. 2(a), for weak alignment/strong active noise (dark blue in upper left) there is a stationary phase where P is approximately zero [54], whereas for strong alignment/weak active noise (bright yellow in lower right) there is a collectively moving phase where P is finite. As shown in Fig. 2(b), fitting of P as a function of alignment strength suggests that these two phases are separated by a line of second order phase transitions.

To study the translational order in the stationary phase, we carry out a larger simulation with system size 256×256 . The total number of time steps is 2×10^6 and simulation samples are collected every 2000 steps in

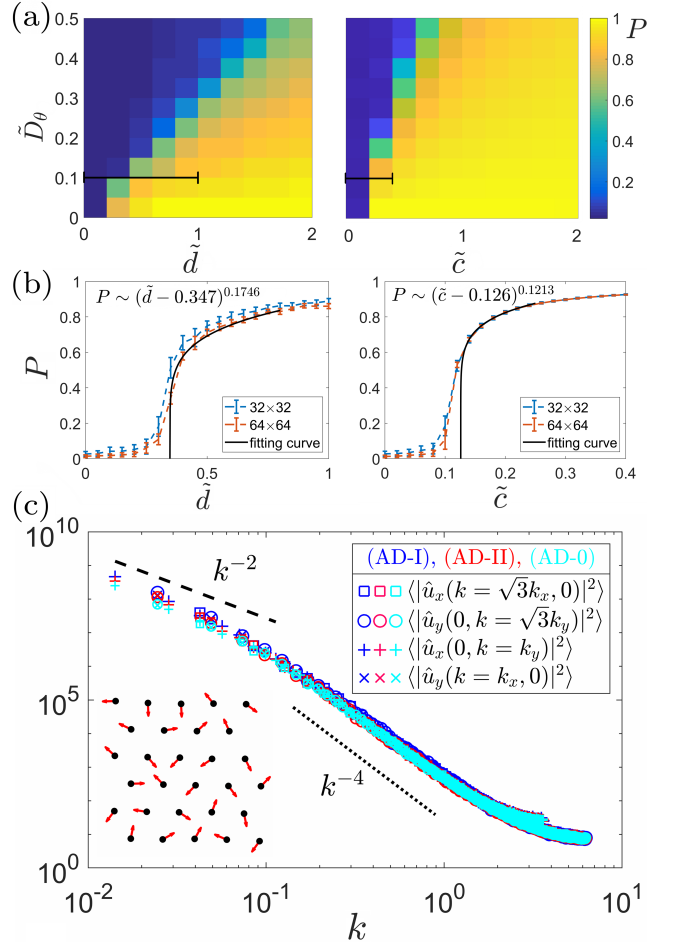


FIG. 2: (a) Phase diagram of AD-I (left) and AD-II (right). Vertical axis: dimensionless noise strength \tilde{D}_θ ; horizontal axis: dimensionless alignment \tilde{d} (AD-I) or \tilde{c} (AD-II). The color represents velocity order parameter P , defined in the main text. (b) Velocity order parameter as a function of alignment, suggesting second-order phase transitions. Left (AD-I), right (AD-II). (c) Log-log plot of the phonon correlation functions $\langle |\hat{u}_x|^2 \rangle$ and $\langle |\hat{u}_y|^2 \rangle$ of the stationary phase along the \hat{k}_x and \hat{k}_y axis, with parameters: $\tilde{b} = 2$, $\tilde{D} = 0.01$, $\tilde{D}_\theta = 0.3$, $(\tilde{\kappa}, \tilde{d}) = (100, 0.1)$ in AD-I, $(\tilde{\kappa}, \tilde{c}) = (20, 0.1)$ in AD-II, and $(\tilde{\kappa}, \tilde{d}, \tilde{c}) = (100, 0, 0)$ in AD-0. Bottom left inset: active forces of the stationary phase.

the steady state. We Fourier transform the phonon field, and compute averages of their norm squared: $\langle |\hat{u}_x(\mathbf{k})|^2 \rangle$, $\langle |\hat{u}_y(\mathbf{k})|^2 \rangle$, which are often called as *phonon correlation functions* (in momentum space). The technical details of numerical computation are presented in SI Sec. II. In Fig. 2(c) we plot $\langle |\hat{u}_x(\mathbf{k})|^2 \rangle$ and $\langle |\hat{u}_y(\mathbf{k})|^2 \rangle$ along \hat{k}_x and \hat{k}_y directions in \mathbf{k} space, and both for AD-I and for AD-II in log-log scale. For comparison we also plot the corresponding result for the model without any alignment (AD-0), which corresponds to $\tilde{d} = \tilde{c} = 0$ in Eqs. (AD-I) and (AD-II). It is remarkable that all curves collapse onto each other, and exhibit k^{-4} scaling in the intermediate length scale ($0.1 < k < 1$). This signifies anomalously large structure fluctuations in the length scales

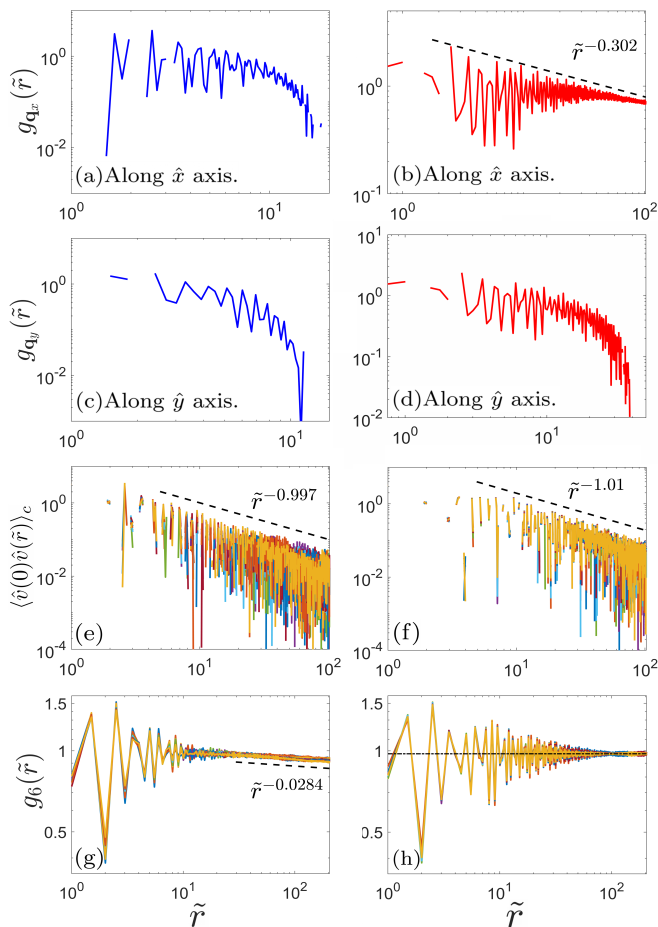


FIG. 3: (a)-(d) Translational correlation functions; (e) & (f) velocity correlation functions; (g) & (h) bond-orientational correlation functions. Left column: AD-I, right volume: AD-II. The parameters are $\bar{D}_\theta = 0.05$, $(\bar{\kappa}, \bar{d}) = (100, 10)$ for AD-I and $(\bar{\kappa}, \bar{c}) = (20, 1)$ for AD-II. We start from an initial state with perfect triangular lattice and $\theta_k = 0$. Data are collected after the system reaches a steady state with $P \approx 0.9915$ in AD-I and $P \approx 0.9830$ in AD-II.

$6a_0 < \ell < 60a_0$ (a_0 the lattice constant) which are caused by the fluctuations of active forces. These results strongly suggest that alignment does not play a role in the stationary phase. For smaller k the phonon correlation functions crossover to k^{-2} scaling, indicating a QLR translation order, in consistent with the result obtained in Ref. [20].

We are however most interested in the collective moving phase. For this purpose, we study the translational correlation function $g_{\mathbf{q}}(\tilde{r})$, velocity correlation function $\langle \hat{v}(0)\hat{v}(\tilde{r}) \rangle_c$, and the bond-orientational correlation function $g_6(\tilde{r})$, all of which are defined in SI Sec. III. In particular, $g_{\mathbf{q}}(\tilde{r})$, defined in Eq. (12) of SI Sec. III, characterizes the correlation of translational order with Bragg vector \mathbf{q} at two regions separated by a dimensionless distance $\tilde{r} \equiv r/a_0$ [55]. As demonstrated in Ref. [44], because of sample-to-sample fluctuations of crystal structure, the Bragg peak \mathbf{q} used for $g_{\mathbf{q}}(\tilde{r})$ must be identified carefully for each sample state. In Fig. 3(a) & (c) we plot

$g_{\mathbf{q}}(\tilde{r})$ for AD-I along \hat{x} and \hat{y} axes for a typical state of the moving phase, which clearly decays faster than power law. Hence there is only short-range (SR) translational order in the moving phase of AD-I. The corresponding results for AD-II are shown in Fig. 3(b) & (d), where it is seen that $g_{\mathbf{q}}(\tilde{r})$ decays algebraically along the \hat{x} axis, and decays faster along the \hat{y} axis. In Fig. 3(e) & (f) we show that velocity correlation functions decay in power-law, which indicate QLRO of velocity field for both AD-I and AD-II. As displayed in Fig. 4(c) & (d) of SI Sec. III, we also find QLRO for the director correlation of active forces. Furthermore, it appears that the exponent of all these power-law scalings are very close to unity. In Fig. 3(g) & (h), we show that the bond-orientational correlation function $g_6(\tilde{r})$ decays in power law for AD-I and converges to a finite limit for AD-II. Hence the bond orientational order is quasi-long ranged for AD-I and long-ranged for AD-II.

In summary, the moving phase of AD-I exhibits QLRO both in velocity and in bond-orientation, but only has SR translational order. Hence it should be categorized as a *moving hexatic phase*. By contrast, the moving phase of AD-II exhibits QLRO in velocity and LRO in bond-orientation, yet the translation order is quasi-long ranged along the moving direction and short ranged in the other direction. This resembles the active smectic phase [45, 46], even though there is no visible layer structures in our system. These numerical results indicate that there is no enhancement of velocity order due to translation order. On the other hand, alignment interactions tend to destabilize translational order in active crystals, and that the destabilizing effect is stronger for Vicsek-like alignment (AD-I) than for elasticity-based alignment (AD-II).

Analytic treatment Our lattice model of active crystal can be coarse-grained to yield a continuous theory in terms of phonon fields $\mathbf{u}(\mathbf{r}, t)$ and director field $\theta(\mathbf{r}, t)$. Detailed analyses is given by SI Sec. IV. Further linearizing, the elastic force Eq. (2) becomes

$$\begin{cases} F_x = (\lambda + 2\mu)\partial_x^2 u_x + \mu\partial_y^2 u_x + (\lambda + \mu)\partial_x \partial_y u_y, \\ F_y = (\lambda + 2\mu)\partial_y^2 u_y + \mu\partial_x^2 u_y + (\lambda + \mu)\partial_x \partial_y u_x, \end{cases} \quad (3)$$

where λ, μ are two Lamé coefficients characterizing the solid elasticity. The dynamics of AD-I is described by:

$$\begin{cases} \gamma \dot{u}_x = F_x + \sqrt{2\gamma T} \xi_x \\ \gamma \dot{u}_y = b\theta + F_y + \gamma\sqrt{2D} \xi_y \\ \dot{\theta} = d\Delta\theta + \sqrt{2D_\theta} \eta \end{cases} \quad (4)$$

where $\xi_x(\mathbf{r}, t), \xi_y(\mathbf{r}, t), \eta(\mathbf{r}, t)$ are all unit Gaussian white noises. We Fourier transform Eqs. (4), and calculate the steady state correlation function for $\mathbf{u}(\mathbf{k}, t)$ and $\theta(\mathbf{k}, t)$:

$$\langle |\hat{u}_x(\mathbf{k})|^2 \rangle = \frac{W_1(\alpha)}{k^6} + \frac{W_2(\alpha)}{k^2}, \quad (5a)$$

$$\langle |\hat{u}_y(\mathbf{k})|^2 \rangle = \frac{W_3(\alpha)}{k^6} + \frac{W_4(\alpha)}{k^2}, \quad (5b)$$

$$\langle |\hat{\theta}(\mathbf{k})|^2 \rangle = \frac{D_\theta}{dk^2}, \quad (5c)$$

where $\alpha = \tan^{-1}(k_y/k_x)$ is the polar angle of \mathbf{k} , and the functions $W_i(\alpha)$, $i = 1, 2, 3, 4$ are defined in Eqs. (28) of SI Sec. IV. While $W_2(\alpha)$, $W_3(\alpha)$, $W_4(\alpha)$ are all positive,

$$W_1(\alpha) = \frac{b^2 D_\theta (d\gamma + 4\lambda) \sin^2 2\alpha}{12d\lambda(d^2\gamma^2 + 4d\gamma\lambda + 3\lambda^2)}. \quad (6)$$

vanishes along \hat{k}_x and \hat{k}_y axes, where $\alpha = 0, \pi/2, \pi, 3\pi/2$ respectively. Hence along these axes, $\langle |\hat{u}_x(\mathbf{k})|^2 \rangle$ scales as k^{-2} instead of k^{-6} along other directions.

The real space fluctuations of phonon fields and director field can be obtained by integrating Eqs. (5) over \mathbf{k} . Integreating Eq. (5c) we see that $\langle \theta(\mathbf{r}, t)^2 \rangle$, diverges logarithmically with system size, and hence the active force exhibits QLRO. Since the velocity is massively coupled to the active force, it should also exhibit QLRO, as demonstrated by our numerical simulation. On the other hand, Integrating Eqs. (5a), (5b) we see that $\langle u_x(\mathbf{r}, t)^2 \rangle$ and $\langle u_y(\mathbf{r}, t)^2 \rangle$ diverge in power law with system size, indicating SR translation orders. These results again agree with our numerical observations shown in Fig. 3.

The dynamics of AD-II in the linearized continuous theory can be similarly obtained:

$$\begin{cases} \gamma \dot{u}_x = F_x + \gamma\sqrt{2D} \xi_x \\ \gamma \dot{u}_y = b\theta + F_y + \gamma\sqrt{2D} \xi_y \\ \dot{\theta} = cF_y + \sqrt{2D_\theta} \eta \end{cases} \quad (7)$$

The steady state correlation functions, calculated in detail in SI Sec. IV, turn out to be more complicated. Here we only display the leading order terms for small k :

$$\langle |\hat{u}_x(\mathbf{k})|^2 \rangle = \frac{W_5(\alpha)}{k^2} + \mathcal{O}(k^0), \quad (8a)$$

$$\langle |\hat{u}_y(\mathbf{k})|^2 \rangle = \frac{W_6(\alpha)}{k^4} + \mathcal{O}(k^{-2}), \quad (8b)$$

$$\langle |\hat{\theta}(\mathbf{k})|^2 \rangle = \frac{W_7(\alpha)}{k^2} + \mathcal{O}(k^0), \quad (8c)$$

where $W_5(\alpha)$, $W_6(\alpha)$, $W_7(\alpha)$ are all positive definite. Since Eq. (8c) scales the same as Eq. (5c) we see that the velocity order is again quasi-long ranged. Integrating Eqs. (8a), (8b) we see that that translational order for AD-II is QLR along x axis and SR along y axis, again consistent with the numerical results displayed in Fig. 3. In SI Sec. V we compare the contour plots of analytical and numerical correlation functions in \mathbf{k} plane for both active dynamics, see quantitative agreements.

To achieve better understanding of our model of active solids, we can generalize the analytic theory to arbitrary d dimensions. The elasticity of a d dimensional isotropic

		Stationary Phase		Moving Phase			
		\mathbf{u}	ψ_6	\mathbf{u}_\parallel	\mathbf{u}_\perp	\mathbf{v}	ψ_6
2D	AD-I	QLRO	LRO	SRO	SRO	QLRO	QLRO
	AD-II	QLRO	LRO	QLRO	SRO	QLRO	LRO
3D	AD-I	LRO	LRO	SRO	SRO	LRO	LRO
	AD-II	LRO	LRO	LRO	SRO	LRO	LRO

TABLE I: Stability of translational order, bond-orientational orders, and velocity order in active crystals in 2D and 3D. In the stationary phase, bond-orientational order is always long-ranged whereas velocity is always short-ranged.

solid can be obtained by adapting Eq. (3), if we replace u_y and ∂_y by \mathbf{u}_\perp and ∇_\perp where \perp denotes the subspace perpendicular to the moving direction \hat{x} , replace θ by $\delta\hat{n}_\perp$, the fluctuation of active force director in the perpendicular subspace. Equations (4) and (7) can be similarly generalized to d dimensions. In SI Sec. VI, an explicit derivation is given for the case $d = 3$. The correlation functions for the phonon fields and for the director fluctuation $\delta\hat{n}_\perp$ can be similarly computed, and the results are still given by Eqs. (5) and (8), as long as u_y are replaced by \mathbf{u}_\perp and θ by $\delta\hat{n}_\perp$. Hence we conclude that for Vicsek-like alignment (AD-I), the translational order of active crystal has critical dimension $d_c^t = 6$, whilst the velocity order has critical dimension $d_c^v = 2$. By contrast, for elasticity-based alignment (AD-II), the translational order along the moving direction has critical dimension $d_c^{t,\parallel} = 2$, and that perpendicular to the moving direction has critical dimension $d_c^{t,\perp} = 4$, whilst the velocity order has critical dimension $d_c^v = 2$. The nature of bond-orientational order however can not be easily determined from our analytic theory. Nonetheless, given our 2D results, we deduce the bond orientational order is long-range above two dimensions both for AD-I and AD-II. The nature of various orders for 2d and 3d cases are summarized in Table I.

In this work, we have provided a complete characterization of various orders in active solids. To test our theoretical results using experiments, sufficiently large system sizes must be prepared and studied. Both the permanent springs and the alignment interaction may, for instance, be realized by remote sensing between nano-robotics [47–49]. It is also conceivable to manipulate self-propelled colloidal particles [50, 51] or link swimmers using polymers and to induce alignment interaction using hydrodynamic effects or magnetic interactions. It would be more interesting to study whether the phases we discovered are related to those solid-like moving structures observed in Vicsek-type models with short-range interactions [21, 22]. These questions will be explored in a future work.

X.X. acknowledge support from NSFC via grant #11674217, as well as additional support from a Shanghai Talent Program. This research is also supported

by Shanghai Municipal Science and Technology Major Project (Grant No.2019SHZDZX01).

* Electronic address: xxing@sjtu.edu.cn

- [1] John Toner, Yuhai Tu, and Sriram Ramaswamy. Hydrodynamics and phases of flocks. *Annals of Physics*, 318(1):170–244, 2005.
- [2] Sriram Ramaswamy. The mechanics and statistics of active matter. *Annual Review of Condensed Matter Physics*, 1(1):323–345, 2010.
- [3] Tamás Vicsek and Anna Zafeiris. Collective motion. *Physics reports*, 517(3-4):71–140, 2012.
- [4] M Cristina Marchetti, Jean-François Joanny, Sriram Ramaswamy, Tanniemola B Liverpool, Jacques Prost, Madan Rao, and R Aditi Simha. Hydrodynamics of soft active matter. *Reviews of Modern Physics*, 85(3):1143, 2013.
- [5] Francesco Ginelli. The physics of the vicsek model. *The European Physical Journal Special Topics*, 225(11):2099–2117, 2016.
- [6] Hugues Chaté. Dry aligning dilute active matter. *Annual Review of Condensed Matter Physics*, 11:189–212, 2020.
- [7] N David Mermin and Herbert Wagner. Absence of ferromagnetism or antiferromagnetism in one-or two-dimensional isotropic heisenberg models. *Physical Review Letters*, 17(22):1133, 1966.
- [8] T. Vicsek, A. Czirók, E. Ben-jacob, I. Cohen, and O. Shochet, Novel Type of Phase Transition in a System of Self-Driven Particles, *Phys. Rev. Lett.*, 75, 1226 (1995).
- [9] John Toner and Yuhai Tu. Long-range order in a two-dimensional dynamical xy model: how birds fly together. *Physical review letters*, 75(23):4326, 1995.
- [10] John Toner. Reanalysis of the hydrodynamic theory of fluid, polar-ordered flocks. *Physical Review E*, 86(3):031918, 2012.
- [11] Yuhai Tu, John Toner, and Markus Ulm. Sound waves and the absence of galilean invariance in flocks. *Physical review letters*, 80(21):4819, 1998.
- [12] Guillaume Grégoire and Hugues Chaté. Onset of collective and cohesive motion. *Physical review letters*, 92(2):025702, 2004.
- [13] John Toner and Yuhai Tu. Flocks, herds, and schools: A quantitative theory of flocking. *Physical review E*, 58(4):4828, 1998.
- [14] Hugues Chaté, Francesco Ginelli, and Raúl Montagne. Simple model for active nematics: Quasi-long-range order and giant fluctuations. *Physical review letters*, 96(18):180602, 2006.
- [15] Sriram Ramaswamy, R Aditi Simha, and John Toner. Active nematics on a substrate: Giant number fluctuations and long-time tails. *EPL (Europhysics Letters)*, 62(2):196, 2003.
- [16] Shradha Mishra and Sriram Ramaswamy. Active nematics are intrinsically phase separated. *Physical review letters*, 97(9):090602, 2006.
- [17] Francesco Ginelli, Fernando Peruani, Markus Bär, and Hugues Chaté. Large-scale collective properties of self-propelled rods. *Physical review letters*, 104(18):184502, 2010.
- [18] Christoph A Weber, Timo Hanke, J Deseigne, S Léonard, Olivier Dauchot, Erwin Frey, and Hugues Chaté. Long-range ordering of vibrated polar disks. *Physical review letters*, 110(20):208001, 2013.
- [19] Biplab Bhattacharjee and Debasish Chaudhuri. Reentrant phase separation in nematically aligning active polar particles. *Soft matter*, 15(42):8483–8495, 2019.
- [20] Christoph A Weber, Christopher Bock, and Erwin Frey. Defect-mediated phase transitions in active soft matter. *Physical review letters*, 112(16):168301, 2014.
- [21] Aitor Martín-Gómez, Demian Levis, Albert Díaz-Guilera, and Ignacio Pagonabarraga. Collective motion of active brownian particles with polar alignment. *Soft matter*, 14(14):2610–2618, 2018.
- [22] Elena Sese-Sansa, Ignacio Pagonabarraga, and Demian Levis. Velocity alignment promotes motility-induced phase separation. *EPL (Europhysics Letters)*, 124(3):30004, 2018.
- [23] Shradha Mishra, R Aditi Simha, and Sriram Ramaswamy. A dynamic renormalization group study of active nematics. *Journal of Statistical Mechanics: Theory and Experiment*, 2010(02):P02003, 2010.
- [24] Suraj Shankar, Sriram Ramaswamy, and M Cristina Marchetti. Low-noise phase of a two-dimensional active nematic system. *Physical Review E*, 97(1):012707, 2018.
- [25] Hal Tasaki. Hohenberg-mermin-wagner-type theorems for equilibrium models of flocking. *Physical Review Letters*, 125(22):220601, 2020.
- [26] Demian Levis, Ignacio Pagonabarraga, and Albert Díaz-Guilera. Synchronization in dynamical networks of locally coupled self-propelled oscillators. *Physical Review X*, 7(1):011028, 2017.
- [27] Guillaume Grégoire, Hugues Chaté, and Yuhai Tu. Moving and staying together without a leader. *Physica D: Nonlinear Phenomena*, 181(3-4):157–170, 2003.
- [28] Isaac Theurkauff, Cécile Cottin-Bizonne, Jérémie Palacci, Christophe Ybert, and Lydric Bocquet. Dynamic clustering in active colloidal suspensions with chemical signaling. *Physical review letters*, 108(26):268303, 2012.
- [29] Ivo Buttinoni, Julian Bialké, Felix Kümmel, Hartmut Löwen, Clemens Bechinger, and Thomas Speck. Dynamical clustering and phase separation in suspensions of self-propelled colloidal particles. *Physical review letters*, 110(23):238301, 2013.
- [30] Jeremie Palacci, Stefano Sacanna, Asher Preska Steinberg, David J Pine, and Paul M Chaikin. Living crystals of light-activated colloidal surfers. *Science*, 339(6122):936–940, 2013.
- [31] Yaouen Fily and M Cristina Marchetti. Athermal phase separation of self-propelled particles with no alignment. *Physical review letters*, 108(23):235702, 2012.
- [32] Julian Bialké, Hartmut Löwen, and Thomas Speck. Microscopic theory for the phase separation of self-propelled repulsive disks. *EPL (Europhysics Letters)*, 103(3):30008, 2013.
- [33] Gabriel S Redner, Michael F Hagan, and Aparna Baskaran. Structure and dynamics of a phase-separating active colloidal fluid. *Physical review letters*, 110(5):055701, 2013.
- [34] Julian Bialké, Thomas Speck, and Hartmut Löwen. Crystallization in a dense suspension of self-propelled particles. *Physical review letters*, 108(16):168301, 2012.
- [35] Ananyo Maitra and Sriram Ramaswamy. Oriented active solids. *Physical Review Letters*, 123(23):238001, 2019.

- [36] Xiangjun Xing and Leo Radzihovsky. Thermal fluctuations and anomalous elasticity of homogeneous nematic elastomers. *EPL (Europhysics Letters)*, 61(6):769, 2003.
- [37] Xiangjun Xing and Leo Radzihovsky. Nonlinear elasticity, fluctuations and heterogeneity of nematic elastomers. *Annals of Physics*, 323(1):105–203, 2008.
- [38] Mark Warner and Eugene Michael Terentjev. *Liquid crystal elastomers*, volume 120. Oxford university press, 2007.
- [39] Eliseo Ferrante, Ali Emre Turgut, Marco Dorigo, and Cristián Huepe. Elasticity-based mechanism for the collective motion of self-propelled particles with springlike interactions: A model system for natural and artificial swarms. *Physical review letters*, 111(26):268302, 2013.
- [40] Eliseo Ferrante, Ali Emre Turgut, Marco Dorigo, and Cristian Huepe. Collective motion dynamics of active solids and active crystals. *New Journal of Physics*, 15(9):095011, 2013.
- [41] Tamás Vicsek, András Czirók, Eshel Ben-Jacob, Inon Cohen, and Ofer Shochet. Novel type of phase transition in a system of self-driven particles. *Physical review letters*, 75(6):1226, 1995.
- [42] Cristián Huepe, Eliseo Ferrante, Tom Wenseleers, and Ali Emre Turgut. Scale-free correlations in flocking systems with position-based interactions. *Journal of Statistical Physics*, 158(3):549–562, 2015.
- [43] Peter E Kloeden and Eckhard Platen. *Numerical solution of stochastic differential equations*, volume 23. Springer Science & Business Media, 2013.
- [44] Yan-Wei Li and Massimo Pica Ciamarra. Accurate determination of the translational correlation function of two-dimensional solids. *Physical Review E*, 100(6):062606, 2019.
- [45] Tapan Chandra Adhyapak, Sriram Ramaswamy, and John Toner. Live soap: stability, order, and fluctuations in apolar active smectics. *Physical review letters*, 110(11):118102, 2013.
- [46] Leiming Chen, John Toner, et al. Universality for moving stripes: A hydrodynamic theory of polar active smectics. *Physical review letters*, 111(8):088701, 2013.
- [47] Ali E Turgut, Hande Çelikkanat, Fatih Gökçe, and Erol Şahin. Self-organized flocking in mobile robot swarms. *Swarm Intelligence*, 2(2-4):97–120, 2008.
- [48] Hande Çelikkanat and Erol Şahin. Steering self-organized robot flocks through externally guided individuals. *Neural Computing and Applications*, 19(6):849–865, 2010.
- [49] Eliseo Ferrante, Ali Emre Turgut, Nithin Mathews, Mauro Birattari, and Marco Dorigo. Flocking in stationary and non-stationary environments: a novel communication strategy for heading alignment. In *International conference on parallel problem solving from nature*, pages 331–340. Springer, 2010.
- [50] Marjolein N Van Der Linden, Lachlan C Alexander, Dirk GAL Aarts, and Olivier Dauchot. Interrupted motility induced phase separation in aligning active colloids. *Physical review letters*, 123(9):098001, 2019.
- [51] François A Lavergne, Hugo Wendehenne, Tobias Bäuerle, and Clemens Bechinger. Group formation and cohesion of active particles with visual perception-dependent motility. *Science*, 364(6435):70–74, 2019.
- [52] Note however in this work the dynamic equations contain no noise term.
- [53] Note that in the original Vicsek model [41], swimmers control their velocities instead of active forces. In the over-damped regime, this difference is inessential.
- [54] It is never strictly zero because the system is finite and there are always instantaneous fluctuations at each time.
- [55] Here the orientation of real space displacement is averaged over. The directionality of $g_{\mathbf{q}}(\tilde{r})$ is carried by the Bragg vector \mathbf{q} . For details, see SI Sec. III.

Supplementary Information

Alignment Destabilizes Crystal Orders in Active Systems

Chen Huang¹, Leiming Chen², and Xiangjun Xing^{1,3,4*}

¹ *Wilczek Quantum Center, School of Physics and Astronomy,
Shanghai Jiao Tong University, Shanghai 200240 China*

² *School of Materials Science and Physics,
China University of Mining and Technology, Xuzhou, Jiangsu, 221116 China*

³ *T.D. Lee Institute, Shanghai Jiao Tong University, Shanghai 200240 China*

⁴ *Shanghai Research Center for Quantum Sciences, Shanghai 201315 China*

PACS numbers:

*Electronic address: xxing@sjtu.edu.cn

I. DIMENSIONLESS FORM OF THE EQUATIONS OF MOTION AND THE CHOICE OF PARAMETERS

We derive in this section the dimensionless equations of the model and specify the parameters used in simulation. To distinguish the coefficients used in simulation with their counterparts in analytical results, we temporarily add a subscript or superscript L (meaning “Lattice”) in this section.

In the simulation model, the space and time units are chosen as a_0 (lattice constant) and τ_0 (the value of τ_0 would be determined later). The dimensionless control parameters are:

$$\begin{aligned} \tilde{b}_L &\equiv b\tau_0/(\gamma a_0), & \tilde{\kappa} &\equiv \kappa\tau_0/\gamma, & \tilde{D}^L &\equiv D\tau_0/a_0^2, & \tilde{D}_\theta^L &\equiv D_\theta\tau_0, & \tilde{d}_L &\equiv d\tau_0, & \tilde{c}_L &\equiv c\gamma a_0, \\ \tilde{\mathbf{F}}_k &\equiv \mathbf{F}_k\tau_0/(\gamma a_0), & \tilde{\eta}_k &\equiv \eta\sqrt{\tau_0}, & \tilde{\xi}_k &\equiv \hat{\xi}\sqrt{\tau_0}. \end{aligned} \quad (1)$$

The dimensionless equation of Eq. (1) is,

$$\dot{\tilde{\mathbf{r}}}_k(\tilde{t}) = \tilde{b}_L \hat{n}(\theta_k) + \tilde{\mathbf{F}}_k(\tilde{t}) + \sqrt{2\tilde{D}^L} \tilde{\xi}_k(\tilde{t}), \quad (2)$$

The dimensionless equations of the two alignment dynamics become:

$$\dot{\theta}_k(\tilde{t}) = \tilde{d}_L (\hat{n}(\theta_k) \times \langle \hat{n} \rangle_k) \cdot \hat{z} + \sqrt{2\tilde{D}_\theta^L} \tilde{\eta}_k, \quad (\text{AD-I}) \quad (3)$$

$$\dot{\theta}_k(\tilde{t}) = \tilde{c}_L (\hat{n}(\theta_k) \times \tilde{\mathbf{F}}_k) \cdot \hat{z} + \sqrt{2\tilde{D}_\theta^L} \tilde{\eta}_k, \quad (\text{AD-II}) \quad (4)$$

We numerically integrate the above dynamic equations using the first-order Euler-Maruyama scheme [1]. We choose $\tau_0 \equiv 0.01a_0^2/D^L$ to ensure the perturbation assumption such that the magnitude of the noise $\sqrt{\tilde{D}^L} = 0.1$ is small compared to the active force and the elastic force. The other parameters are chosen as:

$$\tilde{b}_L = 2, \quad \tilde{\kappa} = 100 \text{ for AD-I, } \tilde{\kappa} = 20 \text{ for AD-II.} \quad (5)$$

In determining the phase diagram, we use a relatively small lattice of size 32×32 to save computational resources, start from a perfect triangular lattice with all active forces orienting randomly.

In studying the translational order and other correlation functions, we use a larger lattice of size 256×256 . For the stationary phase, we choose the parameters $\tilde{D}_\theta^L = 0.3$, $\tilde{d} = 0.1$ for both AD-I and AD-II, and start from a perfect triangular lattice and all active forces orienting randomly. For the collective moving phase, we use the parameter $\tilde{D}_\theta^L = 0.05$ (Note

that by our choice, the magnitude of the angular noise also satisfies the small perturbation condition ($\sqrt{\tilde{D}_\theta^L} < 1$), $\tilde{d} = 10$ for AD-I and $\tilde{d} = 1$ for AD-II, and also start from a perfect lattice, but with all active forces orienting toward the \hat{x} axis. Note that for any finite-size lattice, the average velocity of the collectively moving crystal would slowly change, so we redirect it back toward the \hat{x} axis right after each sample has been collected but before the subsequent simulation steps start.

In the coarse-grained continuous model, using the space and time units a_0 and τ_0 , we obtain the reduced quantities:

$$\begin{aligned} \tilde{b} &\equiv \frac{b\tau_0}{\gamma a_0}, \quad \tilde{\mathbf{F}} \equiv \frac{\mathbf{F}\tau_0}{\gamma a_0}, \quad \begin{pmatrix} \tilde{\mu} \\ \tilde{\lambda} \end{pmatrix} \equiv \frac{\tau_0}{\gamma a_0^2} \begin{pmatrix} \mu \\ \lambda \end{pmatrix}, \quad \tilde{D} \equiv \frac{D\tau_0}{a_0^2}, \quad \tilde{D}_\theta \equiv D_\theta\tau_0, \\ \tilde{d} &\equiv \frac{d\tau_0}{a_0^2}, \quad \tilde{c} \equiv c\gamma a_0, \quad \begin{pmatrix} \tilde{\eta} \\ \tilde{\xi} \end{pmatrix} \equiv \sqrt{\tau_0} \begin{pmatrix} \eta \\ \xi \end{pmatrix}. \end{aligned} \quad (6)$$

The dimensionless form of Eq. (4) is:

$$\dot{\tilde{\mathbf{u}}}(\tilde{\mathbf{r}}, \tilde{t}) = \tilde{b}\theta\hat{y} + \tilde{\mathbf{F}}(\tilde{\mathbf{r}}, \tilde{t}) + \sqrt{2\tilde{D}}\hat{\xi}(\tilde{\mathbf{r}}, \tilde{t}). \quad (7)$$

The two coarse-grained dimensionless alignment dynamics are, respectively,

$$\dot{\theta}(\tilde{\mathbf{r}}, \tilde{t}) = \tilde{d}\tilde{\Delta}\theta + \sqrt{2\tilde{D}_\theta}\tilde{\eta}(\tilde{\mathbf{r}}, \tilde{t}), \quad (\text{AD-}\tilde{\text{I}}') \quad (8)$$

$$\dot{\theta}(\tilde{\mathbf{r}}, \tilde{t}) = \tilde{c}(\hat{n} \times \tilde{\mathbf{F}}) \cdot \hat{z} + \sqrt{2\tilde{D}_\theta}\tilde{\eta}(\tilde{\mathbf{r}}, \tilde{t}). \quad (\text{AD-}\tilde{\text{II}}') \quad (9)$$

where $\tilde{\Delta} \equiv a_0^2\Delta$. Since the linearized elasticity theory in the continuous model also applies to the two-dimensional hexagonal crystal used in our simulation [2], we may relate the *Lamé* constants and the elastic constant via $\tilde{\lambda} = \tilde{\mu} = \tilde{\kappa}\sqrt{3}/4$ [3] in order to compare the two models.

II. FOURIER TRANSFORM ON NON-ORTHOGONAL LATTICE

The simulations use a triangular lattice with rhomb-like boundary, where the lattice points are shown in Fig. 1(a) as the solid black points. We wish to implement the Fourier Transform (FT) to the data (e.g., the displacement u_x , u_y , and the angle θ) sampled on

this triangular lattice into the reciprocal k -space. Although it is easy to implement FT on a square lattice by using the Fast Fourier Transform (FFT) techniques, no direct method exists for Ft on a triangular lattice. However, the triangular lattice can be deemed as originating from a linear transform of the square lattice. Since FT is also a linear transform, we expect a combination of the two linear transforms may serve our purpose. Below is a derivation of this process.

Suppose we sample a complex function $f : \mathbb{R}^n \rightarrow \mathbb{C}$ on a set of n -dimensional points $\Lambda \in \mathbb{R}^n$ in real space. Let $\Phi : \mathbb{R}^n \rightarrow \mathbb{R}^n$ be a linear isomorphic map under which n -dimensional integers are mapped to n -dimensional real values such that $\mathbb{Z}^n \rightarrow \Lambda$. We may obtain the FT of f in terms of the FT of $(f \circ \Phi)$, which is a function on \mathbb{Z}^n . The FT of $(f \circ \Phi)$ is,

$$\mathcal{F}(f \circ \Phi)(s) \equiv \int f \circ \Phi(x) e^{-2\pi i \langle s, x \rangle} dx \quad (10)$$

$$\begin{aligned} &= \frac{1}{|\det \Phi|} \int f(y) e^{-2\pi i \langle \Phi^{-T} s, y \rangle} dy \\ &= \frac{1}{|\det \Phi|} \mathcal{F}(f) (\Phi^{-T} s) \end{aligned} \quad (11)$$

Here a substitution $y = \Phi x$ was made, and it was used that $\langle s, \Phi^{-1} y \rangle = \langle \Phi^{-T} s, y \rangle$. Note that the conventions with respect to the sign of the exponent and factors of 2π may differ.

We now discuss the meaning of the above formula. The function $f \circ \Phi$ is the value of the sample points of f arranged in an n -dimensional array lying on a *standard grid* (equal-axis orthogonal grid). Its Fourier transform gives an array of the same shape, but the interpretation is different: the value at index s in reality is the value at $\Phi^{-T} s \in \mathbb{R}^n$ in k -space, differed by a multiplier $|\det \Phi|$.

In our simulation's setup, $n = 2$ and $\Lambda \in \mathbb{R}^2$ is the set of the triangular lattice points in real space. The function f whose FT we want to compute, can be the displacement field

u_x, u_y or the orientation field θ . The linear map $\mathbf{y} = \Phi \mathbf{x}$ with $\Phi = \begin{pmatrix} 1 & \frac{1}{2} \\ 0 & \frac{\sqrt{3}}{2} \end{pmatrix}$ transforms

a square regular lattice with lattice constant a_0 into the desired triangular lattice with the

same lattice constant. The transverse of its inverse is $\Phi^{-T} = \begin{pmatrix} 1 & 0 \\ -\frac{1}{\sqrt{3}} & \frac{2}{\sqrt{3}} \end{pmatrix}$. The function $f \circ \Phi$

takes the value of the sample points of f on Λ , but its arguments lie on the corresponding

square lattice points. We apply FFT on this real space square lattice (standard grid), obtain its FT values on a k -space square lattice (standard grid) indexed by s , and assign the FT values to its true coordinate in k -space by left multiplying Φ^{-T} to s . Suppose the standard grid in real space has a linear size $L \times L$ and each dimension is divided into equally spaced n points with distance of unity $a_0 = 1$, then there are $n \times n$ total sample points in both real and k -space.

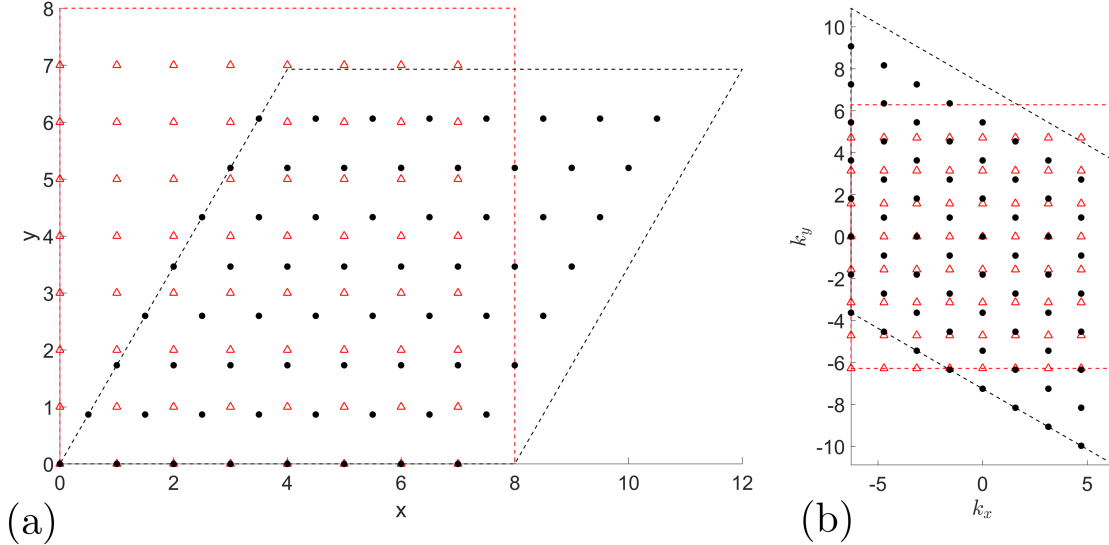


FIG. 1: A lattice with lattice constant $a_0 = 1$ and $L = 8$. The black points denote (a) Sample points in real space and (b) the corresponding k -space points. The red triangles are the standard grid in each space respectively. The dashed lines denote the boundary of the simulation box.

In Fig. 1, a lattice of $L = 8$ and $n = 8$ is shown. The lattice constant of the standard grid in real space is $a_0 = 1$ and that in k -space is $\Delta k = 2\pi/L = \pi/4$. The k -space vector of the standard grid with the minimal magnitude $\mathbf{s}_1 = (0, \frac{2\pi}{L})$ transforms to the true k -space coordinate, $\mathbf{g}_1 = (0, \frac{2\pi}{L} \frac{2}{\sqrt{3}})$, while $\mathbf{s}_2 = (\frac{2\pi}{L}, 0)$ transforms to $\mathbf{g}_2 = (\frac{2\pi}{L}, -\frac{1}{\sqrt{3}} \frac{2\pi}{L})$ with both $|\mathbf{g}_i| = \frac{2\pi}{L} \frac{2}{\sqrt{3}}$.

III. TRANSLATIONAL CORRELATION, PAIR CORRELATION, AND BOND-ORIENTATIONAL CORRELATION

In this section, we discuss the definition and evaluation of the translational correlation, pair correlation of velocity and director of active force, and bond-orientational correlation

in AD-I and AD-II dynamics. For simplicity, the quantities such as r and \mathbf{q} in this section all refer to dimensionless variables.

We first follow the steps in Ref. [4] by defining the translational correlation function as:

$$g_{\mathbf{q}}(r) = \frac{1}{2\pi r \Delta r \rho N} \sum_{j \neq k} \zeta(r - |\mathbf{r}_j - \mathbf{r}_k|) \text{Re}(e^{i\mathbf{q} \cdot (\mathbf{r}_j - \mathbf{r}_k)}). \quad (12)$$

where $\zeta = 1$ if $|\mathbf{r}_j - \mathbf{r}_k|$ is in the region $r \sim r + \Delta r$, otherwise $\zeta = 0$. The number density $\rho = (\sqrt{3}/2)^{-1}$ is the inverse of the area of a unit cell in the triangular lattice of unit length.

We choose \mathbf{q} by evaluating the Bragg peaks of the structure factor

$$Q(q_x, q_y) = \frac{1}{N} \langle \rho(q_x, q_y) \rho(-q_x, -q_y) \rangle, \quad (13)$$

where

$$\rho(q_x, q_y) = \sum_{j=1}^N \exp[i(q_x x_j + q_y y_j)], \quad (14)$$

with x_j and y_j the Cartesian coordinates of the j th particle. The choice of \mathbf{q} should be carefully decided from simulation results, i.e., the true peak value is numerically evaluated around the Bragg peak of a perfect hexagonal lattice $\mathbf{q}_x = (4\pi, 0)$ along the \hat{x} axis, $\mathbf{q}_y = (0, 2\pi \cdot (\sqrt{3}/2)^{-1})$ along the \hat{y} axis, and $\mathbf{q}_t = 2\pi(1, 1/\sqrt{3})$ along a tilted direction.

In Fig. 2 and Fig. 3, we plot $Q(q_x, q_y)$ (the first column) and the corresponding translational correlation function (the second column in Log-Log scale and the third in Log-Linear scale) of typical sample configurations, for AD-I with $(\tilde{\kappa}, \tilde{d}_L) = (100, 10)$ and AD-II with $(\tilde{\kappa}, \tilde{c}_L) = (20, 1)$, respectively. Data is collected after the system has reached a steady state of collective moving, with $P \approx 0.9915$ in AD-I and $P \approx 0.9830$ in AD-II. In AD-I, the translational correlation function decays faster than power law along the wave vector \mathbf{q}_x , \mathbf{q}_y and \mathbf{q}_t , indicating short-range order. However, in AD-II, it has a power law decay along the \hat{x} axis, and exhibits short-range order along \mathbf{q}_y and \mathbf{q}_t .

In the first row of Fig. 4, we show the correlation function of the director of active force in k-space $\langle |\hat{\theta}|^2 \rangle$. We observe a k^{-2} decay in AD-I, and a k^{-2} decay followed by a constant in AD-II. These scaling properties match with the analytical results Eqn. (35) and (41) given in Appendix D.

In the second row of Fig. 4, we plot 10 independent samples at different times of the the pair correlation function of the director of active force,

$$\langle \hat{n}(0) \cdot \hat{n}(r) \rangle = \frac{1}{2\pi r \Delta r \rho N} \sum_{j \neq k} \zeta(r - |\mathbf{r}_j - \mathbf{r}_k|) (\hat{n}_j \cdot \hat{n}_k). \quad (15)$$

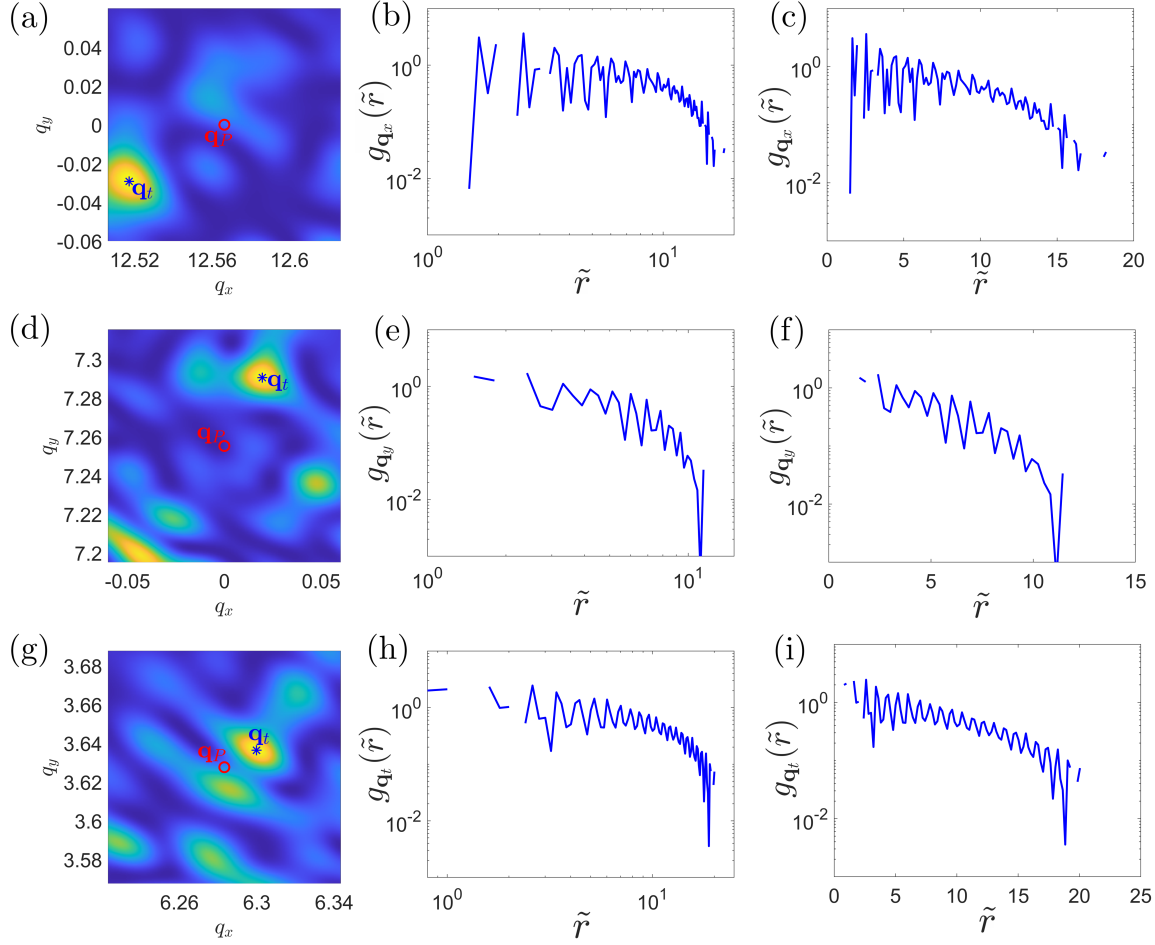


FIG. 2: Bragg peak of $Q(q_x, q_y)$ and the corresponding translational correlation function in AD-I with (a)-(c) $\mathbf{q}_x = (12.5172, -0.0292)$; (d)-(f) $\mathbf{q}_y = (0.0196, 7.2905)$; (g)-(i) $\mathbf{q}_t = (6.2998, 3.6363)$. The second column is in Log-Log scale, while the third column is in Log-Linear scale.

Note we have subtracted the asymptotic value of $\langle \hat{n}(0) \cdot \hat{n}(r) \rangle$ at large enough distance $\langle \hat{n}(0) \cdot \hat{n}(\infty) \rangle$ in the steady state, i.e., $\langle \hat{n}(0) \cdot \hat{n}(r) \rangle_c \equiv \langle \hat{n}(0) \cdot \hat{n}(r) \rangle - \langle \hat{n}(0) \cdot \hat{n}(\infty) \rangle$. We find a power-law decay with exponent being approximately -1 indicating quasi-long range order. A similar treatment is applied to the velocity with

$$\langle \hat{v}(0) \cdot \hat{v}(r) \rangle = \frac{1}{2\pi r \Delta r \rho N} \sum_{j \neq k} \zeta(r - |\mathbf{r}_j - \mathbf{r}_k|) (\hat{v}_j \cdot \hat{v}_k). \quad (16)$$

where the velocity \mathbf{v}_i of each particle is defined by subtracting the coordinates in the two configurations separated by time interval $100\Delta\tilde{t}$, i.e., $\mathbf{v}_i(\tilde{t}) \equiv [\mathbf{r}_i(\tilde{t}) - \mathbf{r}_i(\tilde{t} - 100\Delta\tilde{t})]/(100\Delta\tilde{t})$ and $\hat{v}_i \equiv \mathbf{v}_i/|\mathbf{v}_i|$. We also define and plot the value $\langle \hat{v}(0) \cdot \hat{v}(r) \rangle_c \equiv \langle \hat{v}(0) \cdot \hat{v}(r) \rangle - \langle \hat{v}(0) \cdot \hat{v}(\infty) \rangle$ as shown in Fig. 3(e)-(f) in the main text. The result gives a power-law decay of similar

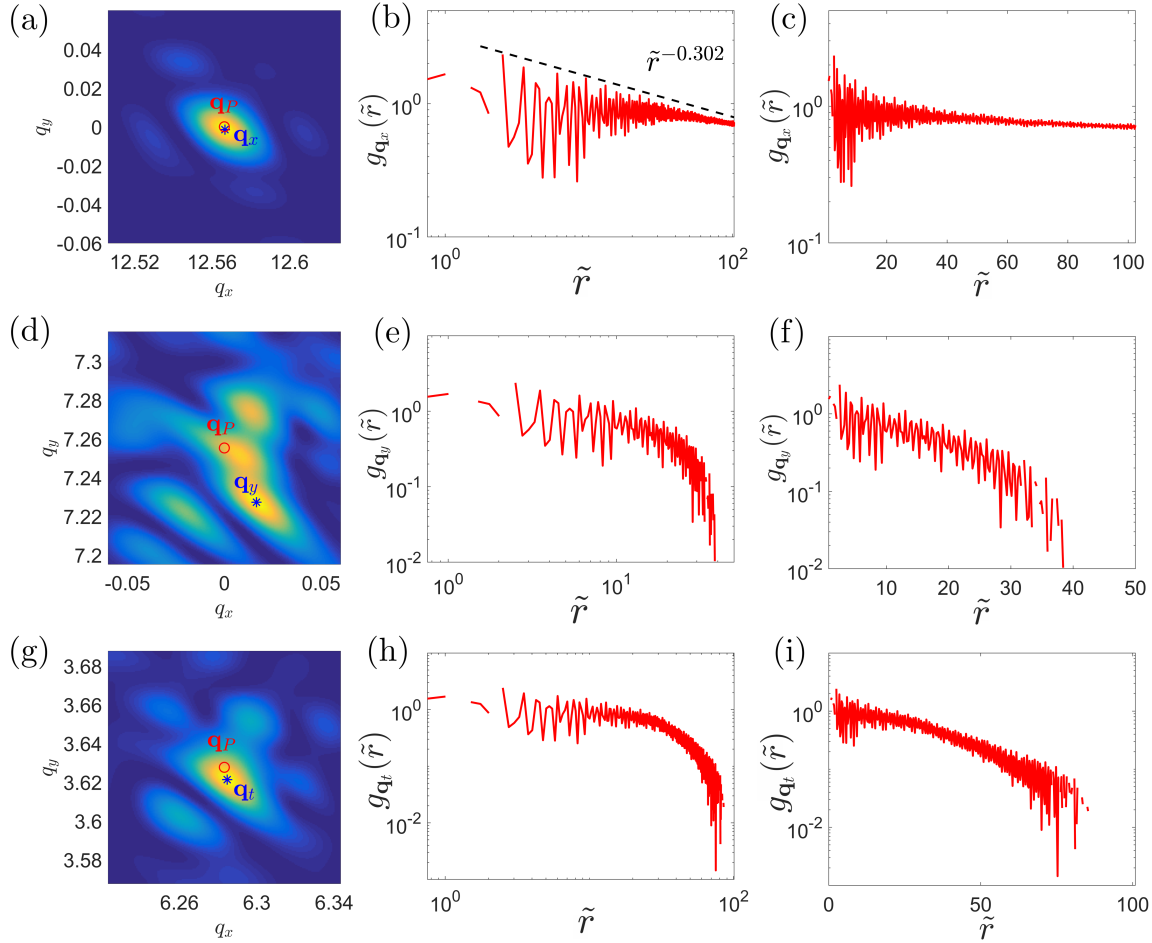


FIG. 3: Bragg peak of $Q(q_x, q_y)$ and the corresponding translational correlation function in AD-II with (a)-(c) $\mathbf{q}_x = (12.5667, -0.0015)$; (d)-(f) $\mathbf{q}_y = (0.0166, 7.2272)$; (g)-(i) $\mathbf{q}_t = (6.2847, 3.6213)$. The second column is in Log-Log scale, while the third column is in Log-Linear scale.

exponents with the director of active force.

In Fig. 4(e)-(f), we show the bond-orientational correlation function [4]:

$$g_6(r) = \text{Re} \langle \psi_6(\vec{r}_i) \psi_6^*(\vec{r}_j) \rangle \equiv \frac{1}{2\pi r \Delta r \rho N} \sum_{j \neq k} \zeta(r - |\mathbf{r}_j - \mathbf{r}_k|) \text{Re}(\psi_6(\vec{r}_i) \psi_6^*(\vec{r}_j)), \quad (17)$$

where $r = |\vec{r}_i - \vec{r}_j|$. The local-bond orientational parameter is defined as $\psi_6(\vec{r}_j) = \frac{1}{n} \sum_{m=1}^n \exp i(6\theta_m^j)$ where the sum runs over the n Voronoi neighbors of the particle, and θ_m^j is the angle of $(\vec{r}_m - \vec{r}_j)$ relative to any fixed axis. In Fig. 4(e)-(f), $g_6(r)$ in AD-I has a power law decay with a non-zero but small exponent -0.0284 . This exponent is obtained from linear fitting of the average of 10 independent sample curves at different simulation steps, after the system has reached the steady state. The value of $g_6(r)$ in AD-II approaches

a constant at large distances. From the numerical results we may conclude that the bond-orientational order in AD-I is QLRO and that in AD-II is LRO. We leave the verification of these predictions and the evaluation of a more accurate power-law exponent to future studies.

IV. ANALYTICAL SOLUTION OF THE CORRELATION FUNCTIONS

To obtain a more thorough understanding of these numerical results, and also to understand analogous systems in higher dimensions, we resort to analytical approach. Our lattice model of active crystal can be coarse-grained to yield a continuous theory that is amenable for analytic study. Let \mathbf{r} be the Lagrange coordinate for a generic swimmer which denotes its position in the initial reference state, $\mathbf{u}(\mathbf{r}, t)$ the phonon field characterizing its displacement from the uniformly moving state, the swimmer's position at time t is then $\mathbf{r} + \mathbf{u}(\mathbf{r}, t) + \mathbf{v}_0 t$, where $\mathbf{v}_0 = b/\gamma$ is the mean velocity as determined from Eq. (1) in the main text (Hence our analytic results apply to the moving phase). The elastic force $\mathbf{F}(\mathbf{r}, t)$ acting on the swimmer at \mathbf{r} can be expressed in terms of $\mathbf{u}(\mathbf{r}, t)$ using the linearized elasticity theory [5, 6]:

$$\mathbf{F} = \mu \nabla^2 \mathbf{u} + (\lambda + \mu) \nabla (\nabla \cdot \mathbf{u}), \quad (18a)$$

where λ and μ are two *Lamé* coefficients. This result is the coarse-grained version of Eq. (2) in the main text. In terms of components we have

$$\begin{cases} F_x = (\lambda + 2\mu) \partial_x^2 u_x + \mu \partial_y^2 u_x + (\lambda + \mu) \partial_x \partial_y u_y, \\ F_y = (\lambda + 2\mu) \partial_y^2 u_y + \mu \partial_x^2 u_y + (\lambda + \mu) \partial_x \partial_y u_x. \end{cases} \quad (18b)$$

The Langevin equations are coarse-grained into stochastic PDEs, which can be further linearized. In particular Eq. (1) in the main text becomes

$$\gamma \dot{\mathbf{u}}(\mathbf{r}, t) = b \theta(\mathbf{r}, t) \hat{y} + \mathbf{F}(\mathbf{r}, t) + \gamma \sqrt{2D} \hat{\xi}(\mathbf{r}, t). \quad (19)$$

where $\theta(\mathbf{r}, t)$ is the coarse-grained version of $\theta_k(t)$, and $\hat{\xi}(\mathbf{r}, t)$ is a 2d Gaussian white noise satisfying $\langle \xi_i(\mathbf{r}, t) \rangle = 0$, $\langle \xi_i(\mathbf{r}, t) \xi_j(\mathbf{r}', t') \rangle = \delta_{ij} \delta(\mathbf{r} - \mathbf{r}') \delta(t - t')$. The stochastic PDE for the phonon field can be obtained by substituting Eq. (18b) into Eq. (19). Here in Eq. (19) and also below in Eqs. (20), (21), the parameters $b, c, d, \gamma, D, D_\theta$ are in general different from

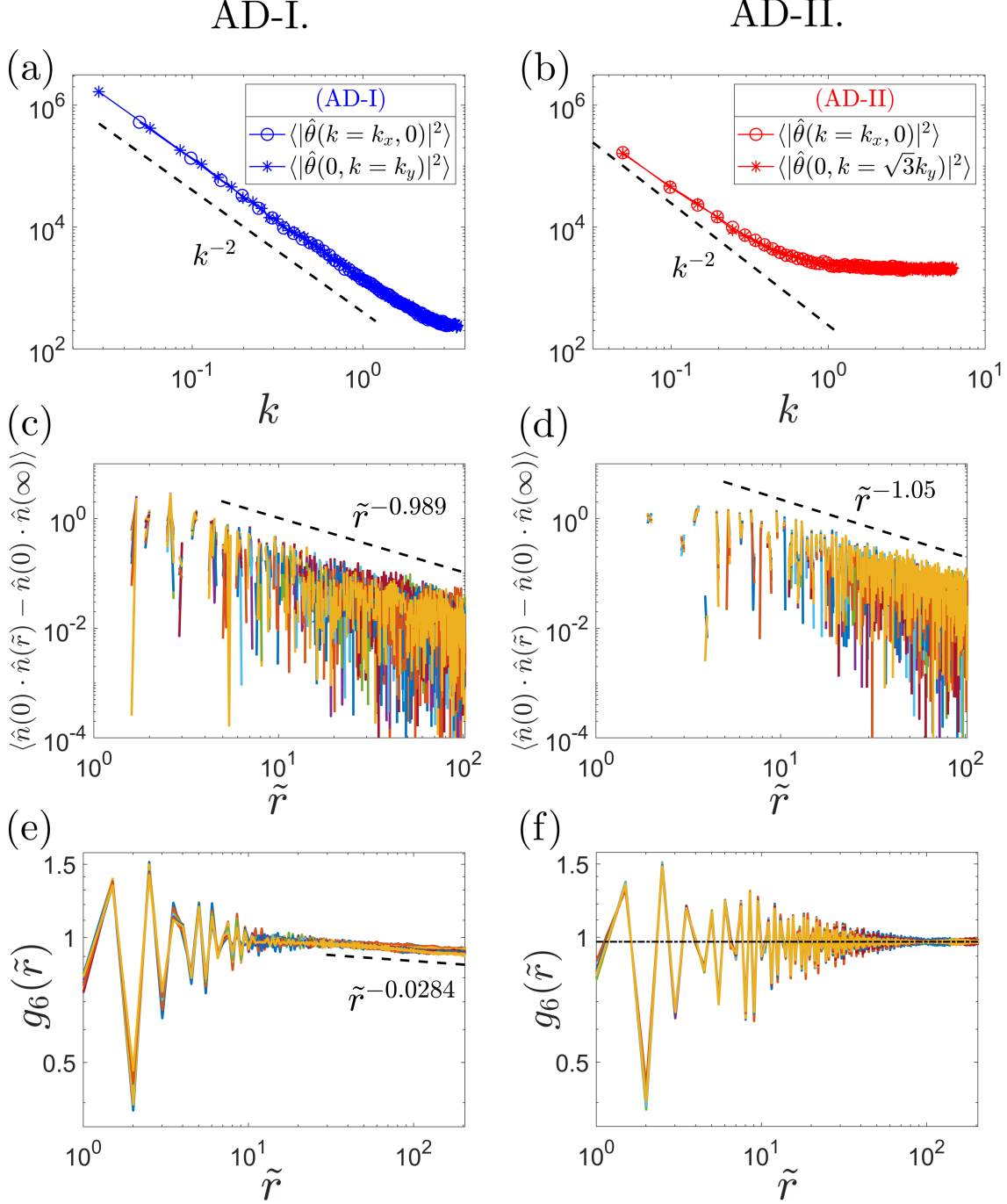


FIG. 4: (a)-(b) The correlation functions $\langle |\hat{\theta}| \rangle$ along \hat{k}_x and \hat{k}_y axis (Note that the k_y value in AD-II is rescaled for comparison according to Eq. (41).), (c)-(d) the pair correlation functions of director of active force, and (e)-(f) the bond-orientational correlation functions of AD-I (the first column) and AD-II (the second column).

their lattice versions in Eqs. (1), (AD-I) and (AD-II) in the main text. We however need not

to be concerned with these differences since we are only interested in the scaling behaviors of correlation functions in the analytic theory.

Coarse-graining and linearizing Eq. (AD-I), we obtain the following set of linearized stochastic PDEs for AD-I:

$$\begin{cases} \gamma \dot{u}_x = F_x + \sqrt{2\gamma T} \xi_x \\ \gamma \dot{u}_y = b\theta + F_y + \gamma\sqrt{2D} \xi_y \\ \dot{\theta} = d\Delta\theta + \sqrt{2D_\theta} \eta \end{cases} \quad (20)$$

where $\eta = \eta(\mathbf{r}, t)$ is a Gaussian white noise satisfying $\langle \eta(\mathbf{r}, t) \rangle = 0$, $\langle \eta(\mathbf{r}, t) \eta(\mathbf{r}', t') \rangle = \delta(\mathbf{r} - \mathbf{r}') \delta(t - t')$. Further carrying out the spatial Fourier transform of Eqs. (20), we obtain linear Langevin equations for $\mathbf{u}(\mathbf{k}, t)$ and $\theta(\mathbf{k}, t)$.

The linearized theory of AD-II can be similarly obtained:

$$\begin{cases} \gamma \dot{u}_x = F_x + \gamma\sqrt{2D} \xi_x \\ \gamma \dot{u}_y = b\theta + F_y + \gamma\sqrt{2D} \xi_y \\ \dot{\theta} = cF_y + \sqrt{2D_\theta} \eta \end{cases} \quad (21)$$

We are now ready to derive the steady state correlation function solution for $\mathbf{u}(\mathbf{k}, t)$ and $\theta(\mathbf{k}, t)$. But before that, let us first consider the solution of a general multidimensional Langevin equation:

$$\dot{\mathbf{x}}(\mathbf{k}, t) + \mathbf{\Gamma} \mathbf{x}(\mathbf{k}, t) = \zeta(\mathbf{k}, t). \quad (22)$$

where $\langle \zeta_i(\mathbf{k}, t) \zeta_j^\dagger(\mathbf{k}', t') \rangle = \langle \zeta_i(\mathbf{k}, t) \zeta_j(-\mathbf{k}', t') \rangle = 2B_{ij} \delta(\mathbf{k} - \mathbf{k}') \delta(t - t')$. The matrices \mathbf{B} and $\mathbf{\Gamma}$ are real, and $\mathbf{x}(\mathbf{k}, t)$ and $\zeta(\mathbf{k}, t)$ are column vectors. Define $\mathbf{y} = e^{\mathbf{\Gamma}t} \mathbf{x}$, it is easy to prove $d\mathbf{y}/dt = e^{\mathbf{\Gamma}t} \zeta$, and we have the formal solution:

$$\mathbf{x}(\mathbf{k}, t) = \int_{-\infty}^t e^{-\mathbf{\Gamma}(t-\tau)} \zeta(\mathbf{k}, \tau) d\tau. \quad (23)$$

The correlation matrix

$$\langle \mathbf{x}(\mathbf{k}, t) \mathbf{x}^\dagger(\mathbf{k}', t') \rangle = \int_{-\infty}^t \int_{-\infty}^{t'} e^{-\mathbf{\Gamma}(t-\tau)} 2\mathbf{B} \delta(\mathbf{k} - \mathbf{k}') \delta(\tau - \tau') e^{-\mathbf{\Gamma}^\dagger(t'-\tau')} d\tau d\tau' \quad (24)$$

$$= \int_{-\infty}^{\min(t, t')} e^{-\mathbf{\Gamma}(t-\tau)} 2\mathbf{B} \delta(\mathbf{k} - \mathbf{k}') e^{-\mathbf{\Gamma}^\dagger(t'-\tau)} d\tau \quad (25)$$

where we used $\mathbf{\Gamma}^\dagger = \mathbf{\Gamma}^T$ in the last equation. Define the autocorrelation matrix as

$$\mathbf{M} \equiv \langle \mathbf{x}(\mathbf{k}, t) \mathbf{x}^\dagger(\mathbf{k}, t) \rangle = \int_{-\infty}^t e^{-\mathbf{\Gamma}(t-\tau)} 2\mathbf{B} e^{-\mathbf{\Gamma}^T(t-\tau)} d\tau \quad (26)$$

we have

$$\mathbf{\Gamma}\mathbf{M} + \mathbf{M}\mathbf{\Gamma}^T = \int_{-\infty}^t e^{-\mathbf{\Gamma}(t-\tau)} 2(\mathbf{\Gamma}\mathbf{B} + \mathbf{B}\mathbf{\Gamma}^T) e^{-\mathbf{\Gamma}^T(t-\tau)} d\tau \quad (27)$$

$$= 2 e^{-\mathbf{\Gamma}t} \left[\int_{-\infty}^t \frac{d}{d\tau} \left(e^{\mathbf{\Gamma}\tau} \mathbf{B} e^{\mathbf{\Gamma}^T\tau} \right) d\tau \right] e^{-\mathbf{\Gamma}t} = 2\mathbf{B} \quad (28)$$

This is a *Lyapunov equation* [7] that can be solved analytically.

In AD-I, after implementing Fourier transform for the spatial component, we obtain the Lyapunov equation:

$$\begin{pmatrix} \dot{\hat{u}}_x \\ \dot{\hat{u}}_y \\ \dot{\hat{\theta}} \end{pmatrix} + \mathbf{\Gamma} \begin{pmatrix} \hat{u}_x \\ \hat{u}_y \\ \hat{\theta} \end{pmatrix} = \begin{pmatrix} \sqrt{2D}\hat{\xi}_x \\ \sqrt{2D}\hat{\xi}_y \\ \sqrt{2D_\theta}\hat{\eta} \end{pmatrix} \quad (29)$$

where

$$\mathbf{\Gamma} = \frac{1}{\gamma} \begin{pmatrix} \lambda(3k_x^2 + k_y^2) & 2\lambda k_x k_y & 0 \\ 2\lambda k_x k_y & \lambda(3k_y^2 + k_x^2) & -b \\ 0 & 0 & \gamma d(k_x^2 + k_y^2) \end{pmatrix} \quad (30)$$

and

$$\mathbf{M} = \begin{pmatrix} \langle |\hat{u}_x|^2 \rangle & \langle \hat{u}_x \hat{u}_y^* \rangle & \langle \hat{u}_x \hat{\theta}^* \rangle \\ \langle \hat{u}_y \hat{u}_x^* \rangle & \langle |\hat{u}_y|^2 \rangle & \langle \hat{u}_y \hat{\theta}^* \rangle \\ \langle \hat{\theta} \hat{u}_x^* \rangle & \langle \hat{\theta} \hat{u}_y^* \rangle & \langle |\hat{\theta}|^2 \rangle \end{pmatrix}, \quad \mathbf{B} = \begin{pmatrix} D & 0 & 0 \\ 0 & D & 0 \\ 0 & 0 & D_\theta \end{pmatrix} \quad (31)$$

The solution is

$$\left\{ \begin{array}{l} \langle |\hat{u}_x(\mathbf{k})|^2 \rangle = \frac{D(k_x^2 + 3k_y^2)\gamma}{3k^4\lambda} + \frac{b^2 D_\theta k_x^2 k_y^2 (d\gamma + 4\lambda)}{3k^{10}\lambda d(d^2\gamma^2 + 4d\gamma\lambda + 3\lambda^2)} \\ \quad \equiv \frac{W_1(\alpha)}{k^6} + \frac{W_2(\alpha)}{k^2}, \\ \langle |\hat{u}_y(\mathbf{k})|^2 \rangle = \frac{D(3k_x^2 + k_y^2)\gamma}{3k^4\lambda} + \frac{b^2 D_\theta [d(3k_x^4 + 3k_x^2 k_y^2 + k_y^4)\gamma + (3k_x^2 + k_y^2)^2 \lambda]}{3k^{10}\lambda d(d^2\gamma^2 + 4d\gamma\lambda + 3\lambda^2)} \\ \quad \equiv \frac{W_3(\alpha)}{k^6} + \frac{W_4(\alpha)}{k^2}, \\ \langle |\hat{\theta}(\mathbf{k})|^2 \rangle = \frac{D_\theta}{dk^2}. \end{array} \right.$$

where $k = \sqrt{k_x^2 + k_y^2}$ and α is the polar angle such that $(k_x, k_y) = k(\cos \alpha, \sin \alpha)$. The constants are:

$$\begin{aligned} W_1(\alpha) &= \frac{b^2 D_\theta (d\gamma + 4\lambda) \sin^2 2\alpha}{12d\lambda(d^2\gamma^2 + 4d\gamma\lambda + 3\lambda^2)}, \\ W_2(\alpha) &= \frac{\gamma D(2 - \cos 2\alpha)}{3\lambda}, \\ W_3(\alpha) &= \frac{b^2 D_\theta [d\gamma(15 + 8 \cos 2\alpha + \cos 4\alpha) + \lambda(36 + 32 \cos 2\alpha + 4 \cos 4\alpha)]}{24d\lambda(d^2\gamma^2 + 4d\gamma\lambda + 3\lambda^2)}, \\ W_4(\alpha) &= \frac{\gamma D(2 + \cos 2\alpha)}{3\lambda}. \end{aligned} \tag{32}$$

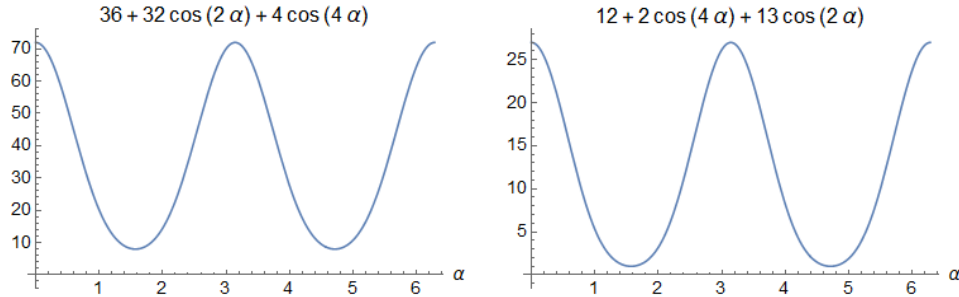


FIG. 5: The functions $W_3(\alpha)$ and $W_5(\alpha)$ are always positive in the interval $[0, 2\pi]$.

It is obvious that all the above coefficients $W_1(\alpha)$, $W_2(\alpha)$, $W_3(\alpha)$ (See Fig. 5), $W_4(\alpha)$ are positive, except that $W_1(\alpha)$ might be zero at $\alpha = 0, \pi/2, \pi, 3\pi/2$. We may conclude that as $k \rightarrow 0$ in AD-I, $\langle |\hat{u}_x|^2 \rangle$ scales as k^{-6} , $\langle |\hat{\theta}|^2 \rangle$ scales as k^{-2} , and $\langle |\hat{u}_y|^2 \rangle$ scales as k^{-4} . However, along the two special orthogonal axis \hat{k}_x ($\alpha = 0$ or π) and \hat{k}_y ($\alpha = \pi/2$ or $3\pi/2$), $\langle |\hat{u}_x|^2 \rangle$ scales as k^{-2} . To be more specific, along the two orthogonal axis \hat{k}_x and \hat{k}_y the correlation functions are,

$$\langle |\hat{u}_x(k_x, 0)|^2 \rangle = \frac{\gamma D}{3\lambda k_x^2}, \quad \langle |\hat{u}_x(0, k_y)|^2 \rangle = \frac{\gamma D}{\lambda k_y^2}, \quad (33)$$

$$\langle |\hat{u}_y(k_x, 0)|^2 \rangle = \frac{b^2 D_\theta}{d\lambda(d\gamma + \lambda)k_x^6} + \frac{\gamma D}{\lambda k_x^2}, \quad \langle |\hat{u}_y(0, k_y)|^2 \rangle = \frac{b^2 D_\theta}{3d\lambda(d\gamma + 3\lambda)k_y^6} + \frac{\gamma D}{3\lambda k_y^2}, \quad (34)$$

$$\langle |\hat{\theta}(k_x, 0)|^2 \rangle = \frac{D_\theta}{dk_x^2}, \quad \langle |\hat{\theta}(0, k_y)|^2 \rangle = \frac{D_\theta}{dk_y^2}. \quad (35)$$

In AD-II, after implementing Fourier Transform to the spatial component, we obtain

$$\begin{pmatrix} \dot{\hat{u}}_x \\ \dot{\hat{u}}_y \\ \dot{\hat{\theta}} \end{pmatrix} + \mathbf{\Gamma} \begin{pmatrix} \hat{u}_x \\ \hat{u}_y \\ \hat{\theta} \end{pmatrix} = \begin{pmatrix} \sqrt{2D} \hat{\xi}_x \\ \sqrt{2D} \hat{\xi}_y \\ \sqrt{2D_\theta} \hat{\eta} \end{pmatrix}. \quad (36)$$

where

$$\mathbf{\Gamma} = \frac{1}{\gamma} \begin{pmatrix} \lambda(3k_x^2 + k_y^2) & 2\lambda k_x k_y & 0 \\ 2\lambda k_x k_y & \lambda(3k_y^2 + k_x^2) & -b \\ 2\gamma\lambda c k_x k_y & \gamma\lambda c(3k_y^2 + k_x^2) & 0 \end{pmatrix}. \quad (37)$$

The solution is

$$\left\{ \begin{aligned} \langle |\hat{u}_x(\mathbf{k})|^2 \rangle &= \frac{b [16D_\theta k_x^2 k_y^2 + c^2 D(k_x^4 + 12k_x^2 k_y^2 + 27k_y^4)\gamma^2] + 12cDk^4(k_x^2 + 3k_y^2)\gamma\lambda}{3ck^4\lambda [bc(k_x^2 + 9k_y^2)\gamma + 12k^4\lambda]} \\ &\equiv \frac{W_5(\alpha)}{k^2} + \mathcal{O}(1), \\ \langle |\hat{u}_y(\mathbf{k})|^2 \rangle &= \frac{3b^2 c D_\theta k^2 \gamma + b(3k_x^2 + k_y^2) [4D_\theta(3k_x^2 + k_y^2) + c^2 D(k_x^2 + 9k_y^2)\gamma^2] \lambda + 12cDk^4(3k_x^2 + k_y^2)\gamma\lambda^2}{3ck^4\lambda^2 [bc(k_x^2 + 9k_y^2)\gamma + 12k^4\lambda]} \\ &\equiv \frac{W_6(\alpha)}{k^4} + \mathcal{O}\left(\frac{1}{k^2}\right), \\ \langle |\hat{\theta}(\mathbf{k})|^2 \rangle &= \frac{b^2 c^2 D_\theta (k_x^2 + 3k_y^2)\gamma^2 + bck^2\gamma [13D_\theta k^2 + c^2 D(k_x^2 + 9k_y^2)\gamma^2] \lambda + 12k^6(D_\theta + c^2\gamma^2 D)\lambda^2}{bck^2\lambda [bc(k_x^2 + 9k_y^2)\gamma + 12k^4\lambda]} \\ &\equiv \frac{W_7(\alpha)}{k^2} + \mathcal{O}(1). \end{aligned} \right.$$

where

$$\begin{aligned} W_5(\alpha) &= \frac{c^2\gamma^2 D(12 + 2\cos 4\alpha + 13\cos 2\alpha) + D_\theta(2 - 2\cos 4\alpha)}{3c^2\gamma\lambda(5 - 4\cos 2\alpha)}, \\ W_6(\alpha) &= \frac{bD_\theta}{c\lambda^2(5 - 4\cos 2\alpha)}, \\ W_7(\alpha) &= \frac{\gamma D_\theta(2 - \cos 2\alpha)}{\lambda(5 - 4\cos 2\alpha)}. \end{aligned} \quad (38)$$

It is obvious that all the coefficients $W_5(\alpha)$ (See Fig. 5), $W_6(\alpha)$ and $W_7(\alpha)$ are always positive. We may conclude that as $k \rightarrow 0$ in AD-II, $\langle |\hat{u}_x|^2 \rangle$ and $\langle |\hat{\theta}|^2 \rangle$ scale as k^{-2} , while $\langle |\hat{u}_y|^2 \rangle$ scales as k^{-4} . Specially, along the two orthogonal axis \hat{k}_x ($\alpha = 0$ or π) and \hat{k}_y ($\alpha = \pi/2$ or $3\pi/2$) the phonon correlation functions are,

$$\langle |\hat{u}_x(k_x, 0)|^2 \rangle = \frac{\gamma D}{3\lambda k_x^2}, \quad \langle |\hat{u}_x(0, k_y)|^2 \rangle = \frac{\gamma D}{\lambda k_y^2}, \quad (39)$$

$$\langle |\hat{u}_y(k_x, 0)|^2 \rangle = \frac{bD_\theta}{c\lambda^2 k_x^4} + \frac{\gamma D}{\lambda k_x^2}, \quad \langle |\hat{u}_y(0, k_y)|^2 \rangle = \frac{bD_\theta}{9c\lambda^2 k_y^4} + \frac{\gamma D}{3\lambda k_y^2}, \quad (40)$$

$$\langle |\hat{\theta}(k_x, 0)|^2 \rangle = \frac{\gamma D_\theta}{\lambda k_x^2} + \frac{D_\theta + c^2 \gamma^2 D}{bc}, \quad \langle |\hat{\theta}(0, k_y)|^2 \rangle = \frac{\gamma D_\theta}{3\lambda k_y^2} + \frac{D_\theta + c^2 \gamma^2 D}{bc}. \quad (41)$$

In the limit of $b = 0$, the phonon correlation functions in both AD-I and AD-II reduce to the same form, which is exactly the phonon correlation of passive crystals:

$$\langle |\hat{u}_x(\mathbf{k})|^2 \rangle = \frac{\gamma D(2 - \cos 2\alpha)}{3\lambda k^2}, \quad (42)$$

$$\langle |\hat{u}_y(\mathbf{k})|^2 \rangle = \frac{\gamma D(2 + \cos 2\alpha)}{3\lambda k^2}. \quad (43)$$

and along the \hat{k}_x and \hat{k}_y axis,

$$\langle |\hat{u}_x(k_x, 0)|^2 \rangle = \frac{\gamma D}{3\lambda k_x^2}, \quad \langle |\hat{u}_x(0, k_y)|^2 \rangle = \frac{\gamma D}{\lambda k_y^2}, \quad (44)$$

$$\langle |\hat{u}_y(k_x, 0)|^2 \rangle = \frac{\gamma D}{\lambda k_x^2}, \quad \langle |\hat{u}_y(0, k_y)|^2 \rangle = \frac{\gamma D}{3\lambda k_y^2}. \quad (45)$$

These results are consistent with the displacement correlation functions of isotropic solids [2]:

$$\langle |\hat{u}_i(\mathbf{k})\hat{u}_j(-\mathbf{k})| \rangle = \frac{T\hat{k}_i\hat{k}_j}{3(\lambda + 2\mu)k^2} + \frac{T(1 - \hat{k}_i\hat{k}_j)}{\mu k^2}, \quad (46)$$

by choosing $\lambda = \mu$ and $i = j$.

V. CONTOUR PLOTS OF THE PHONON CORRELATION FUNCTIONS IN THE COLLECTIVE MOVING PHASE

In Fig. 6 we plot the contour curves of the phonon correlation functions in the collective moving phase in k_x - k_y plane. The parameters are: $\tilde{d}_L = \tilde{d} = 10$ and $\tilde{\kappa} = 100$ for AD-I, $\tilde{c}_L = \tilde{c} = 1$ and $\tilde{\kappa} = 20$ for AD-II, $\tilde{b}_L = \tilde{b} = 2$, $\tilde{D}_\theta^L = \tilde{D}_\theta = 0.05$, $\tilde{\lambda} = \tilde{\mu} = \tilde{\kappa}\sqrt{3}/4$. Note that we let $\tilde{d}_L = \tilde{d}$ even though there is no direct correspondence between these two coefficients. The numerical results are given in the first row within each subplot of Fig. 6

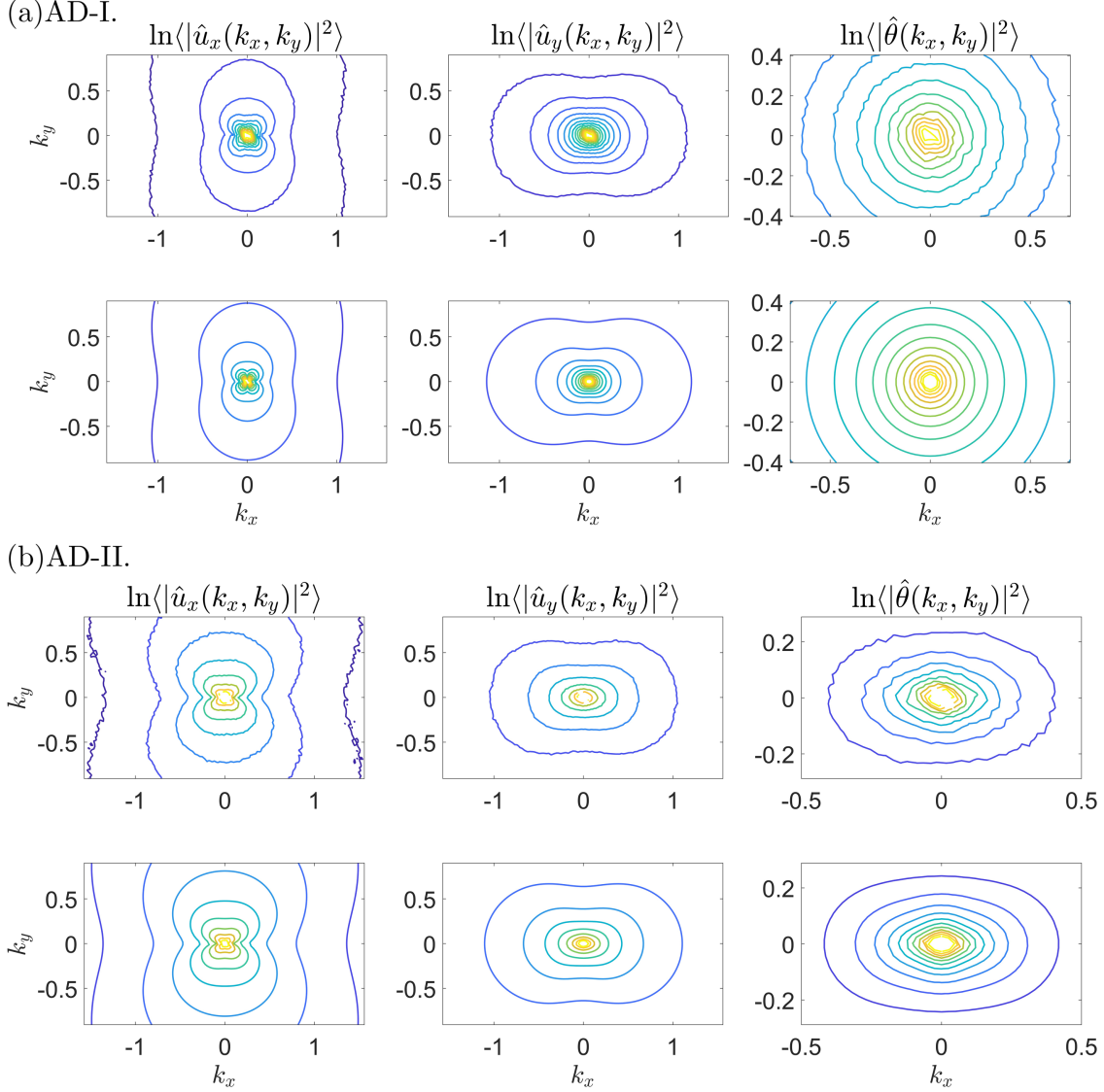


FIG. 6: Contour plot of the logarithm of the phonon correlation functions $\langle|\hat{u}_x|^2\rangle$, $\langle|\hat{u}_y|^2\rangle$ and $\langle|\hat{\theta}|^2\rangle$ in k -space (arbitrary unit) in the Collective Moving phase, obtained from both simulation (first row in each subplot) and theoretical (second row in each subplot) results. (a) AD-I with $\tilde{d} = \tilde{d}_L = 10$. (b) AD-II with $\tilde{c} = \tilde{c}_L = 1$.

and the analytical results in the second row for comparison. The absolute value between the simulation and analytical curves might not be exactly equal, since they may differ by some constants such as the Fourier coefficients during FFT, which however are not of importance for our purpose. It can be seen that the scaling behaviors predicted by theory is consistent with the simulation results. Besides, $\langle|\hat{\theta}|^2\rangle$ in AD-I is rotationally invariant, which originates from the rotational invariance of the active dynamics of θ in AD-I.

VI. GENERALIZATION OF THE EQUATIONS OF MOTION INTO THREE DIMENSIONS

In this section we discuss the analytical treatment of Eq. (3a) in three dimensions, which can be written as

$$F_i = \mu \sum_{j=1}^3 \partial_j^2 u_i + (\lambda + \mu) \sum_{j=1}^3 \partial_i \partial_j u_j \quad (47)$$

or more explicitly as

$$\begin{cases} F_x = \mu(\partial_x^2 u_x + \partial_y^2 u_x + \partial_z^2 u_x) + (\lambda + \mu)(\partial_x^2 u_x + \partial_x \partial_y u_y + \partial_x \partial_z u_z), \\ F_y = \mu(\partial_x^2 u_y + \partial_y^2 u_y + \partial_z^2 u_y) + (\lambda + \mu)(\partial_y \partial_x u_x + \partial_y^2 u_y + \partial_y \partial_z u_z), \\ F_z = \mu(\partial_x^2 u_z + \partial_y^2 u_z + \partial_z^2 u_z) + (\lambda + \mu)(\partial_z \partial_x u_x + \partial_z \partial_y u_y + \partial_z^2 u_z). \end{cases} \quad (48)$$

Under the assumption of $\theta \ll 1$, we may decompose the active force direction into one parallel to the collective moving direction \hat{x} and the other perpendicular to it, i.e., $\hat{n} = \hat{n}_\parallel + \hat{n}_\perp$ where $|\hat{n}_\perp| \ll 1$. We can also decompose the elastic force $\mathbf{F} = \mathbf{F}_\parallel + \mathbf{F}_\perp$. The overdamped dynamics of the displacement field is,

$$\gamma \dot{\mathbf{u}}(\mathbf{r}, t) = b \hat{n}_\perp + \mathbf{F}(\mathbf{r}, t) + \gamma \sqrt{2D} \hat{\xi}(\mathbf{r}, t). \quad (49)$$

where $\hat{\xi}(\mathbf{r}, t)$ is a vector Gaussian white noise satisfying $\langle \xi_i(\mathbf{r}, t) \rangle = 0$, $\langle \xi_i(\mathbf{r}, t) \xi_j(\mathbf{r}', t') \rangle = \delta_{ij} \delta(\mathbf{r} - \mathbf{r}') \delta(t - t')$, and it can be decomposed as $\hat{\xi} = \xi_x \hat{x} + \hat{\xi}_\perp$. The continuum limit of (AD-I) and (AD-II) are respectively,

$$\dot{\hat{n}}_\perp(\mathbf{r}, t) = d \Delta \hat{n}_\perp + \sqrt{2D_\theta} \hat{\eta}_\perp(\mathbf{r}, t), \quad (\text{AD-I}')$$

$$\begin{aligned} \dot{\hat{n}}_\perp(\mathbf{r}, t) &= c (\hat{n} \times \mathbf{F}) \times \hat{n} + \sqrt{2D_\theta} \hat{\eta}_\perp(\mathbf{r}, t) \\ &\approx c \mathbf{F}_\perp + \sqrt{2D_\theta} \hat{\eta}_\perp(\mathbf{r}, t). \end{aligned} \quad (\text{AD-II}')$$

where $\hat{\eta}_\perp(\mathbf{r}, t)$ is a 2d vector Gaussian white noise in the \hat{y} - \hat{z} plane satisfying $\langle \eta_{\perp i}(\mathbf{r}, t) \rangle = 0$, $\langle \eta_{\perp i}(\mathbf{r}, t) \eta_{\perp j}(\mathbf{r}', t') \rangle = \delta_{ij} \delta(\mathbf{r} - \mathbf{r}') \delta(t - t')$.

We can substitute Eq.(48) into Eq.(49) together with Eq.(AD-I'), and obtain the dynamic

equations for AD-I:

$$\begin{cases} \gamma \dot{u}_x = F_x + \gamma\sqrt{2D} \xi_x \\ \gamma \dot{\mathbf{u}}_{\perp} = b \hat{n}_{\perp} + \mathbf{F}_{\perp} + \gamma\sqrt{2D} \hat{\xi}_{\perp} \cdot \\ \dot{\hat{n}}_{\perp} = d \Delta \hat{n}_{\perp} + \sqrt{2D_{\theta}} \hat{\eta}_{\perp} \end{cases} \quad (50)$$

For AD-II, the dynamic equations are given by,

$$\begin{cases} \gamma \dot{u}_x = F_x + \gamma\sqrt{2D} \xi_x \\ \gamma \dot{\mathbf{u}}_{\perp} = b \hat{n}_{\perp} + \mathbf{F}_{\perp} + \gamma\sqrt{2D} \hat{\xi}_{\perp} \cdot \\ \dot{\hat{n}}_{\perp} = c \mathbf{F}_{\perp} + \sqrt{2D_{\theta}} \hat{\eta}_{\perp} \end{cases} \quad (51)$$

It can be easily seen that Eqs. (50) and (51) are direct generalizations of Eqs. (5) and (8) to the 3d case. The above arguments can be easily extended to higher dimensions.

-
- [1] Peter E Kloeden and Eckhard Platen. *Numerical solution of stochastic differential equations*, volume 23. Springer Science & Business Media, 2013.
 - [2] Paul M Chaikin, Tom C Lubensky, and Thomas A Witten. *Principles of condensed matter physics*, volume 10. Cambridge university press Cambridge, 1995.
 - [3] WG Hoover, WT Ashurst, and RJ Olness. Two-dimensional computer studies of crystal stability and fluid viscosity. *The Journal of Chemical Physics*, 60(10):4043–4047, 1974.
 - [4] Yan-Wei Li and Massimo Pica Ciamarra. Accurate determination of the translational correlation function of two-dimensional solids. *Physical Review E*, 100(6):062606, 2019.
 - [5] LD Landau and EM Lifshitz. *Theory of elasticity*. Butterworth-Heinemann, 3rd ed. New York, 1986.
 - [6] Alexander L Fetter and John Dirk Walecka. *Theoretical mechanics of particles and continua*. Courier Corporation, 2003.
 - [7] Aleksandr Mikhailovich Lyapunov. The general problem of the stability of motion. *International journal of control*, 55(3):531–534, 1992.